FINITE DIFFERENCE BEAM PROPAGATION METHOD FOR ANALYZING BEND ENHANCED OPTICAL TOUCH SENSOR

by

Hüseyin Afşer

B.S., in Electrical and Electronics Engineering, Boğaziçi University, 2006

Submitted to the Institute for Graduate Studies in
Science and Engineering in partial fulfillment of
the requirements for the degree of
Master of Science

Graduate Program in Electrical and Electronics Engineering
Boğaziçi University

2008

ACKNOWLEDGEMENTS

I would like to thank to my thesis supervisor Assist. Prof. Heba Yüksel for her guidance and help during the preparation of this dissertion. I would like to mention her tolerance, her excessive help and motivation.

ABSTRACT

FINITE DIFFERENCE BEAM PROPAGATION METHOD FOR ANALYZING BEND ENHANCED OPTICAL TOUCH SENSOR

Analysis of waveguides by computational methods is very important and widely used in optical fiber communications since the power loss due to bending of the optical fibers decreases the channel capacity of the optical fiber links. These systems require proper analysis tools to understand the effects of corruption and degradation of the channel capacity resulting from external disturbances.

Although telecommunication systems tries to analyze the corruption in the optical waveguides such as power attenuation and channel degregation, optical waveguide based sensor applications trie to seek ways of using these changes or corruptions for sensing different properties of the environment. Since optical sensors carry some advantages as being insensitive to electromagnetic interferance , having long durability and high precision; they deserve certain attention.

The aim of this thesis is to provide an analysis method for electrical field and power propagation in waveguides undergoing severe bending by using finite difference beam propagation methods in three dimensions, where the waveguides are bent severely so that the considerable amount of power radiation occurs to the outside of the waveguide with the intention of sensing. As an application in this thesis we propose and analyze a bend enhanced optical touch sensor with the developed three dimensional finite difference beam propagation methods and validate our analysis and reason on the operability of this sensor.

ÖZET

SONLU FARK IŞIN YAYILIM METODUYLA EĞİMLİ OPTİK DOKUNMA SENSÖRÜŇUN ANALİZİ

Fiber optik haberleşme ağlarnda güç kaybı kanalın kapasitesini azalttığı için dalga kılavuzlarının bilgi işlem metotlarıyla analizi çok önemlidir. Bu sistemler, dışardan gelen ve kanalın kapasitesini bozan değişkenlerin etkilerini anlamak için uygun analiz araçlarına ihtiyaç duymaktadır.

Haberleşme sistemleri optik dalga kılavuzlarındaki bozulmann ve güç kaybının analizini yapmaktadır; diğer yandan, optik dalga klavuzuna dayanan sensör uygulamaları ise bu bozulmalardan yola çıkarak çevre değişkenlerini algılamaya yarayan uygulamar bulmaya çalışmaktadır. Optik sensörler bereberinde, elektromanyetik müdahalelere karşı etkisiz olma, uzun ömüre ve yüksek hassasiyete sahip olma gibi çeşitli avantajlar getirdikleri için belli bir ilgiyi haketmektedir.

Bu tezin amacı, üç boyutta sonlu fark ışık yayılım metodlarını kullanarak, dış ortamdan bilgi almak amacyla bükülmüş dalga klavuzlarndaki elektrik ve güç değişimlerini inceleyecek, bir analiz methodu geliştirmektir. Analiz metodunun bir uygulaması ve doğrulaması olarak ise eğimli optik dokunma sensörü incelenmiştir.

TABLE OF CONTENTS

LIST OF FIGURES

LIST OF TABLES

LIST OF SYMBOLS/ABBREVIATIONS

$\mathbf{B}$	Magnetic flux density
$\mathbf{D}$	Electric flux density
$\mathbf{E}$	Electric field intensity
$\mathbf{E}_x$	Electric field vector along x direction
$\mathbf{E}^x_{(m,n)}$	$\mathbf{E}_x$ for mesh point (m, n)
$\mathbf{H}$	Magnetic field intensity
$\mathbf{H}^x$	Magnetic field vector along x direction
$\mathbf{T}$	Transmission coefficient
$\mathbf{R}$	Reflaction coefficient
A_{xx}	Propagation operator, matrix for $\mathbf{E}_x$
A_{yy}	Propagation operator, matrix for $\mathbf{E}_y$
B_{xx}	Propagation operator, matrix for $\mathbf{H}_x$
B_{yy}	Propagation operator, matrix for $\mathbf{H}_y$
k	Free space wavevector
k_x	Wavevector along x direction
$n(m, n, l)$	Refractive index distribution in finite mesh
$n(x, y, z)$	Refractive index distribution in physical space
n_o	Reference refractive index
n_{clad}	Refractive index in the cladding of the waveguide
n_{core}	Refractive index in the core of the waveguide
β_m	Eigenvalue of propagation mode m
λ	Wavelength
ω	Angular frequency
σ	Conductivity
∇	Gradient operator
$\nabla\cdot$	Divergence operator
$\nabla\times$	Curl operator
AWG	Arrayed waveguide gratings
BPM	Beam propagation method

FD	Finite difference
FD	Finite element
TBC	Transparent boundary conditions
PML	Perfectly matching layers
WDM	Wavelength division multiplexing

1. INTRODUCTION

1.1. Background and Overview

During last few decades we have seen an enormous increase in bandwidth requirements for telecom and datacom transmission systems due to the growth of the Internet and excess data transmission. This in turn, has put enormous demands on the lightwave transmission systems and the integrated and fiber optic photonic components that are the foundation of such systems. Conversely, it has been the continual advances in these components as fibers, lasers, detectors, modulators, switches, wavelength demultiplexing devices (WDM's), which have enabled systems to meet these ever increasing demands [1] . These demands require proper analysis and modeling tools to optimize the applications and analyze theirs operation under different conditions.

Apart being useful from information carrying the optical systems find usage as sensor applications as well. Several applications have been reported which use the optical power in the waveguide to sense the environment that the waveguide is interacting with. Bend sensors [2], pressure sensors [3], optical touch sensors [4][5] are some examples that uses optical sensing techniques. However since the applications and uses of optical devices for communication systems outnumber its sensor applications, there is a limited work and analysis for sensor applications.

There are several numerical methods to analyze optical systems. Finite Element (FE) and Finite Difference (FD) methods are the mostly used ones. All of them have pros and cons but one can find an optimum method that suits the application being analyzed.

1.2. Finite Element Method

The Finite Element method [6][7][8], is a powerful numerical technique for the solution of partial differential equations, and it is widely used in different fields of engineering. It is based on partitioning the problem space into a mesh of non overlapping polygonal regions or elements. Triangles and quadrilaterals are two commonly used types of element. Inside each element the solution to the partial differential equation is approximated by polynomial functions, usually corefirst or second order polynomials. The approximate solution needs to satisfy certain constraints, which depend on the particular problem, such as boundary conditions and continuity along the common edges of the elements. A solution is selected from a set of basis functions that obeys these conditions.

The power of the finite element method lies in the flexibility in the choice of mesh. The basic method allows for an enormous variety of meshing strategies. Provided that a suitable automated procedure can be found to partition the problem domain, structures of nearly unrestricted geometry can be handled. This is particularly useful for non-rectangular structures with curved or slanting sections. In addition, it is possible to control the mesh density in order to make use of smaller elements in areas where the solution is changing rapidly (such as corners) and larger elements where it is more uniform. This enables a smaller number of nodes (and therefore less computational resources) to be used to obtain a given level of accuracy. Adaptive meshing techniques are available to perform this optimization.

Finite element methods suffer from its complexity and divergence problems. Certain conditions should be imposed on the mesh in order to prevent unwanted results. Also after proposing and using an initial mesh profile it is not easy to change the setup and apply it to a different geometry.

1.3. Finite Difference Method

Finite Difference Methods are widely used to model the optical systems due to their stability, rather simplicity and accuracy. It can be applied to the scalar, semi or full vector solution to the Maxwell's Equations. Several papers are being reported constantly to perfect their implementation for different applications.

It represent the original problem in a finite mesh grid and approximates the derivatives using the mesh grid. It can be used to analyze different structures and applications so that it is versatile, this is one of the reasons that we have chosen Finite Difference Methods. The problem can be solved using time domain or frequency domain techniques with the accuracy being scalable by the user.

Finite Difference Time Domain methods in three dimensions propagate the beam as a frame after frame collection of vector elements. The electromagnetic equations of the propagation can be scalar, semi vector or full vector solutions. Most of the work in finite difference methods differs as being paraxial or wide angle. Paraxial solutions can not simulate abrupt changes along propagation direction, however wide angle solutions overcome this problem by making higher order approximation to the derivative along the propagation direction.

Since the research field is quite active in terms of applications and analysis methods we see new papers published every year either trying to make the analysis methods faster, more accurate or to explain their optimization for different applications. In this thesis we utilize three dimensional finite difference methods for sensing applications, and give a novel sensor application to demonstrate our analysis as well as application.

1.4. Bend Enhanced Optical Touch Sensor

So far, several touch sensors have been proposed and devised based on the use of surface acoustic waves, piezoelectric transducers, capacitive device, and resistive membranes [9]. However, the acoustic approach requires a high driven electrical power while the piezoelectric and capacitive technologies need to have specially designed electronic circuit to prevent a high output saturation voltage as well as to suppress the unwanted electrostatic inductance change. In addition, humidity and fluctuation of the surrounding temperature are the main factors that limit the life and the performance of these touch sensor technologies. The resistive membrane based touch sensor also has short life because of the movement of the membrane that induces a degree of wear and tear.

Apart from its counterparts, optical touch sensors carriy a lot of advantages that promise their more common usage in the future as a human interface device. These advantages can be summarized as follows:

- They are cheap and can be manufactured easily. Thin plastic optical fibers can be used and be provided for touch sensing applications

- They do not tear or wear out with time so they are durable and they have long usage times.

- They need small activation forces; they do not need periodic calibration.

- They are immune to electromagnetic interference.

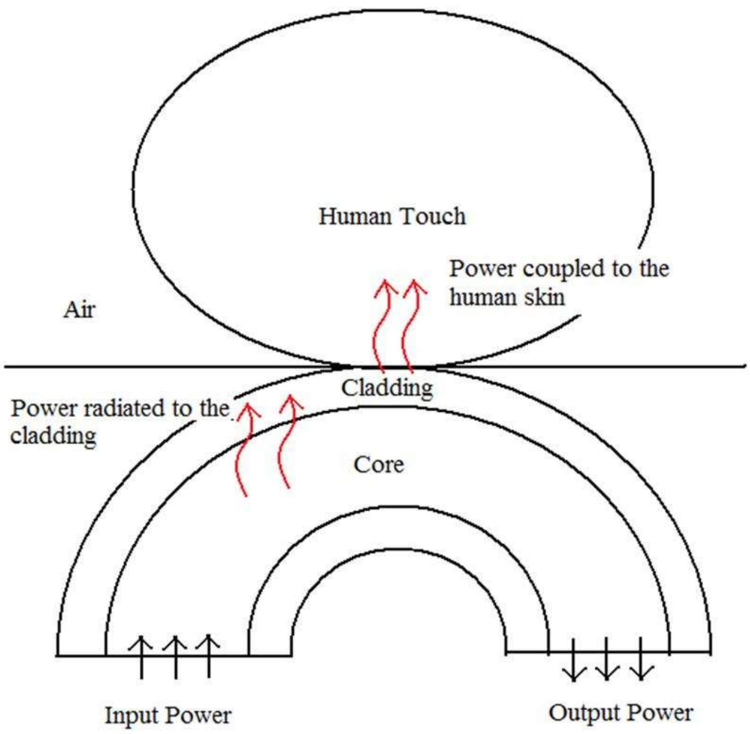

Figure 1.1. Proposed touch sensor topology

The refractive index of the human skin varies between 1.4 and 1.5 [10], which is around the refractive index of the PMMA optical fiber waveguides. Since the refractive index of air is 1, by adjusting the bending radius it is possible to prevent excess power radiation into the air, when there is no touch. Besides, in case of a human touch; it is possible to capture enough power to be detected by the receiver at the end of the fiber. (see Figure 1.1)

The effect of bending is to allow certain amount of power coupling to the cladding. When there is no touching, this power should be maintained in the waveguide and in case of touching it should be coupled to the human skin. This application is also important for other waveguide sensor applications. The problem of power coupling between the core and cladding and using the cladding as a controlled power exchange region is not analyzed in the literature. This thesis aims to analyze this application in an electromagnetic point of view with finite difference beam propagation methods.

2. ELECTROMAGNETIC THEORY

In this chapter, a basic electromagnetic theory background that is necessary to analyze the propagation of light in optical waveguides, is presented. First, Maxwell's equations are explained in isotropic and nonhomogeneous media. Then the common levels of approximation to the solutions of Maxwell's equations, semi vector and full vector solutions are derived by explaining the main differences. Paraxial and wide angle approximations for beam propagation method are explained and the modes of propagation in the waveguides are analyzed. Lastly we explain the conformal transformation to transform curved regions into straight contours.

2.1. Maxwell's Equations

In complex notations, the Maxwell equation for nonhomogeneous media is given as follows [11]:

$$\nabla \times \mathbf{E} = -j\omega\mathbf{B} \tag{2.1}$$

$$\nabla \times \mathbf{H} = j\omega\mathbf{D} \tag{2.2}$$

$$\nabla \cdot \mathbf{D} = 0 \tag{2.3}$$

$$\nabla \cdot \mathbf{H} = 0 \tag{2.4}$$

The vectors **E** and **B** are the electric and magnetic field intensities, **D** and **B** are the electric and magnetic flux densities respectively. A time dependence of the form e^{jwt} is assumed and suppressed from equations hereon. The relationship between angular frequency ω and the wavelength λ is as follows:

$$k = \frac{2\pi c}{\lambda} \tag{2.5}$$

where c is the speed of light. In isotropic media the following relations hold:

$$\mathbf{D} = \epsilon \mathbf{E} \tag{2.6}$$

$$\mathbf{B} = \mu \mathbf{H} \tag{2.7}$$

With the permittivity and permeability values for medium given by:

$$\epsilon = \epsilon_r \epsilon_0 \tag{2.8}$$

$$\mu = \mu_r \mu_0 \tag{2.9}$$

Here ϵ_r and μ_r are the relative permittivity and permeability of the medium and ϵ_0 and$\mu = \mu_r \mu_0$ are the permittivity and permeability of free space respectively. In isotropic medium the permittivity and permeability values are independent of orientation, but in a nonhomogeneous medium they can be a function of the position. For example a graded index waveguide is a good example of an isotropic but nonhomogeneous medium.

The subject of this thesis covers isotropic and non magnetic (μ_r=1) materials. The following definitions of free space wave number k and refractive-index n are used frequently in this thesis. One should also note that the refractive index of free space equals to one.

$$k = \omega \sqrt{\mu_0 \epsilon_0} \tag{2.10}$$

$$n = \sqrt{\epsilon_r} \tag{2.11}$$

2.2. Solutions of Maxwell's Equations

In order to analyze the electromagnetic behavior in optical waveguides Maxwell's equations need to be solved by including the fact that the refractive index of the medium is nonhomogeneous, that is, it depends on the positions in the medium. Throughout this thesis the refractive index will be assumed to be a function of position in rectangular coordinates as $n(x, y, z)$ and the following geometry will be used to solve the equations in three dimensions.

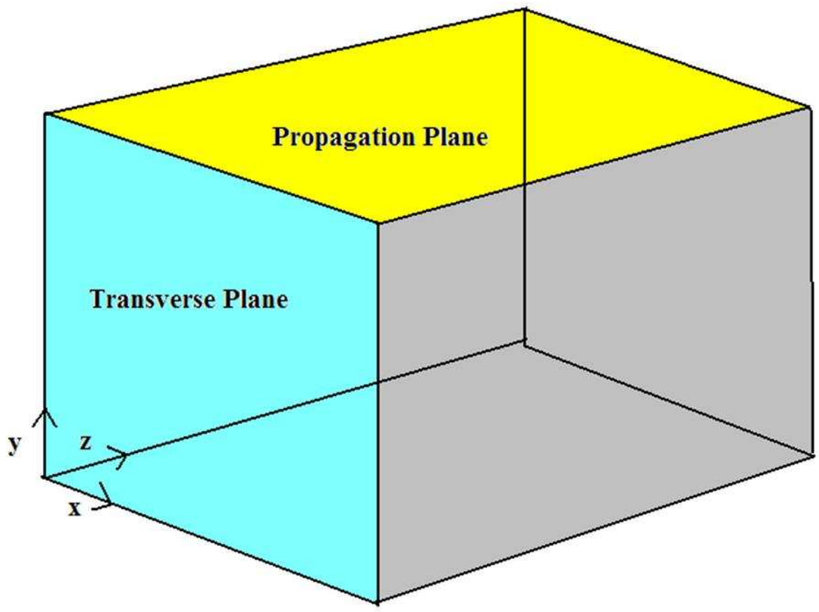

Figure 2.1. Geometry used to solve Maxwell's Equation

Here the propagation is assumed to be in z direction, so that the plane described by x and y axis, is the transverse plane. In order to obtain the governing equations for propagation one has to use the two coupled curl equations Eq. (2.1) and Eq. (2.2) together. By using (2.6), (2.7), (2.11) and noting that μ_r=1 we obtain:

$$\nabla \times \mathbf{E} = -j\omega\mu_0\mathbf{H} \tag{2.12}$$

$$\nabla \times \mathbf{H} = j\omega n^2\epsilon_0\mathbf{E} \tag{2.13}$$

If we use Eq. (2.12) in Eq. (2.13),

$$\nabla \times \nabla \times \mathbf{E} - n^2 k^2 \mathbf{E} = 0 \tag{2.14}$$

If we use the identity [12],

$$\nabla \times \nabla \times = \nabla(\nabla \cdot) - \nabla^2 \tag{2.15}$$

For the electric field we obtain:

$$\nabla(\nabla \cdot \mathbf{E}) - \nabla^2 \mathbf{E} - n^2 k^2 \mathbf{E} = 0 \tag{2.16}$$

By using $\mathbf{E}_t$ as the electric field in transverse plane, $\mathbf{E}_z$ as the electrical field in propagation direction and using the subscript t for vector Laplacian, divergence and gradient operators in order to separate the components of transverse and propagation planes we obtain:

$$\nabla_t \cdot \mathbf{E}_t + n^2 k^2 \mathbf{E}_t = \nabla_t \left(\nabla_t \cdot \mathbf{E}_t + \frac{\partial \mathbf{E}_z}{\partial z} \right) \tag{2.17}$$

If we separate Eq. (2.3) into transverse and propagation components we get,

$$\nabla_t \cdot (n^2 \mathbf{E}_t) + \frac{\partial^2 n^2}{\partial z^2} \mathbf{E}_z + n^2 \frac{\partial \mathbf{E}_z}{\partial z} = 0 \tag{2.18}$$

If the refractive index profile changes slowly in the propagation direction then we can assume:

$$\frac{\partial^2 n^2}{\partial z^2} \mathbf{E}_z \approx 0 \tag{2.19}$$

This assumption allows us to approximate the derivative in z direction with transverse operations as:

$$\frac{\partial \mathbf{E}_z}{\partial z} \approx -\frac{1}{n^2} \nabla_t \cdot (n^2 \mathbf{E}_t) \tag{2.20}$$

If we substitute Eq. (2.20) into Eq. (2.16) we obtain,

$$\nabla^2 \mathbf{E}_t + n^2 k^2 \mathbf{E}_t = \nabla_t \left(\nabla_t \cdot \mathbf{E}_t - \frac{1}{n^2} \nabla_t \cdot (n^2 \mathbf{E}_t) \right) \tag{2.21}$$

This can be written as:

$$\nabla^2 \mathbf{E}_t + n^2 k^2 \mathbf{E}_t = -\nabla_t (\nabla_t \mathtt{ln} n^2 \cdot \mathbf{E}_t) \tag{2.22}$$

If we open the Eq. (2.22) for components of transverse plane in x and y direction we obtain:

$$\nabla^2 \mathbf{E}_x + n^2 k^2 \mathbf{E}_x = -\frac{\partial}{\partial x}\left(\frac{\partial n^2}{\partial x}\mathbf{E}_x\right) - \frac{\partial}{\partial x}\left(\frac{\partial n^2}{\partial y}\mathbf{E}_y\right) \tag{2.23}$$

$$\nabla^2 \mathbf{E}_y + n^2 k^2 \mathbf{E}_y = -\frac{\partial}{\partial y}\left(\frac{\partial n^2}{\partial x}\mathbf{E}_x\right) - \frac{\partial}{\partial y}\left(\frac{\partial n^2}{\partial y}\mathbf{E}_y\right) \tag{2.24}$$

We can write a trial solution for Eq. (2.22) of the form:

$$\mathbf{E}_x = \hat{\mathbf{E}}_x e^{-jn_0 kz} \tag{2.25}$$

where n_0 is a reference refractive index and if we make the slowly varying envelope approximation [13], for the derivatives along propagation direction we get

$$\frac{\partial \mathbf{E}_x}{\partial z} = \frac{\partial \hat{\mathbf{E}}_x}{\partial z} e^{-jn_0 kz} - jn_0 k \hat{\mathbf{E}}_x \tag{2.26}$$

$$\frac{\partial^2 \mathbf{E}_x}{\partial z^2} = \frac{\partial^2 \hat{\mathbf{E}}_x}{\partial z^2} e^{-jn_0kz} - 2jn_0k \frac{\partial \hat{\mathbf{E}}_x}{\partial z} e^{-jn_0kz} - n_0^2 k^2 \hat{\mathbf{E}}_x e^{-jn_0kz} \tag{2.27}$$

In Eq. (2.27) if we assume the change of the first derivative is much bigger than the second derivative as:

$$\left| \frac{\partial^2 \hat{\mathbf{E}}_x}{\partial z^2} \right| << 2n_0k \left| \frac{\partial \hat{\mathbf{E}}_x}{\partial z} \right| \tag{2.28}$$

and factoring out the e^{-jn_0kz} term hereon in our analysis, for $\mathbf{E}_x$ we obtain the paraxial solution as:

$$j \frac{\partial \hat{\mathbf{E}}_x}{\partial z} = A_{xx} \hat{\mathbf{E}}_x + A_{xy} \hat{\mathbf{E}}_y \tag{2.29}$$

Ignoring the second derivative eases the problem and allows us to approximate it with a first order derivative along z direction and transverse derivatives only. Of course it brings limitation to the analysis since the change of electric field is limited to change with only first derivative in the propagation direction. This approximation is known as paraxial solution. The solutions which take into account the second derivative are known as the wide angle solutions, for the paraxial case a fast change of electric field along propagation direction will cause some error.

The derivative operators in Eq. (2.29) are given as:

$$A_{xx}\hat{\mathbf{E}}_x = \frac{1}{2n_0k}\left\{\frac{\partial}{\partial x}\left[\frac{1}{n^2}\frac{\partial}{\partial x}(n^2\hat{\mathbf{E}}_x)\right] + \frac{\partial^2}{\partial y^2}\hat{\mathbf{E}}_x + (n^2 - n_0^2)k^2\hat{\mathbf{E}}_x\right\} \tag{2.30}$$

$$A_{xy}\hat{\mathbf{E}}_y = \frac{1}{2n_0k}\left\{\frac{\partial}{\partial x}\left[\frac{1}{n^2}\frac{\partial}{\partial y}(n^2\hat{\mathbf{E}}_y)\right] - \frac{\partial^2}{\partial x\partial y}\hat{\mathbf{E}}_y\right\} \tag{2.31}$$

Similarly for $\hat{\mathbf{E}}_y$ we get:

$$j\frac{\partial\hat{\mathbf{E}}_y}{\partial z} = A_{yy}\hat{\mathbf{E}}_y + A_{yx}\hat{\mathbf{E}}_x \tag{2.32}$$

$$A_{yy}\hat{\mathbf{E}}_y = \frac{1}{2n_0k}\left\{\frac{\partial}{\partial y}\left[\frac{1}{n^2}\frac{\partial}{\partial y}(n^2\hat{\mathbf{E}}_y)\right] + \frac{\partial^2}{\partial x^2}\hat{\mathbf{E}}_y + (n^2 - n_0^2)k^2\hat{\mathbf{E}}_y\right\} \tag{2.33}$$

$$A_{yx}\hat{\mathbf{E}}_x = \frac{1}{2n_0k}\left\{\frac{\partial}{\partial y}\left[\frac{1}{n^2}\frac{\partial}{\partial x}(n^2\hat{\mathbf{E}}_x)\right] - \frac{\partial^2}{\partial y\partial x}\hat{\mathbf{E}}_x\right\} \tag{2.34}$$

The derivation of the magnetic field $\mathbf{H}$ is similar. Using two coupled curl Eq. (2.1) and (2.2) to solve for $\mathbf{H}$ results in:

$$\nabla\times\nabla\times\mathbf{H} - n^2k^2\mathbf{H} - \frac{1}{n^2}\nabla n^2\times(\nabla\times\mathbf{H}) = 0 \tag{2.35}$$

The transverse components of magnetic field can be approximated by:

$$\nabla^2 \mathbf{H}_x + n^2 k^2 \mathbf{H}_x - \frac{1}{n^2}\frac{\partial n^2}{\partial y}\left(\frac{\partial \mathbf{H}_x}{\partial y} - \frac{\partial \mathbf{H}_y}{\partial x}\right) = 0 \tag{2.36}$$

$$\nabla^2 \mathbf{H}_y + n^2 k^2 \mathbf{H}_y - \frac{1}{n^2}\frac{\partial n^2}{\partial x}\left(\frac{\partial \mathbf{H}_y}{\partial x} - \frac{\partial \mathbf{H}_x}{\partial y}\right) = 0 \tag{2.37}$$

By letting $\mathbf{H}_x = \hat{\mathbf{H}}_x e^{-jn_0kz}$, and making the slowly varying approximation one more time as:

$$\left|\frac{\partial^2 \hat{\mathbf{H}}_x}{\partial z^2}\right| << 2n_0k\left|\frac{\partial \hat{\mathbf{H}}_x}{\partial z}\right| \tag{2.38}$$

We obtain:

$$j\frac{\partial \hat{\mathbf{H}}_x}{\partial z} = B_{xx}\hat{\mathbf{H}}_x + B_{xy}\hat{\mathbf{H}}_y \tag{2.39}$$

$$j\frac{\partial \hat{\mathbf{H}}_y}{\partial z} = B_{yy}\hat{\mathbf{H}}_y + B_{yx}\hat{\mathbf{H}}_x \tag{2.40}$$

Where we can write the differential operators as follows:

$$B_{xx}\hat{\mathbf{H}}_x = \frac{1}{2n_0k}\left\{\frac{\partial^2}{\partial x^2}\hat{\mathbf{H}}_x + (n^2 - n_0^2)k^2\hat{\mathbf{H}}_x + n^2\left[\frac{\partial}{\partial y}\left(\frac{1}{n^2}\frac{\partial\hat{\mathbf{H}}_x}{\partial y}\right)\right]\right\} \tag{2.41}$$

$$B_{yy}\hat{\mathbf{H}}_y = \frac{1}{2n_0k}\left\{\frac{\partial^2}{\partial y^2}\hat{\mathbf{H}}_y + (n^2 - n_0^2)k^2\hat{\mathbf{H}}_y + n^2\left[\frac{\partial}{\partial x}\left(\frac{1}{n^2}\frac{\partial\hat{\mathbf{H}}_y}{\partial x}\right)\right]\right\} \tag{2.42}$$

$$B_{xy}\hat{\mathbf{H}}_y = \frac{1}{2n_0k}\left\{\frac{\partial^2}{\partial y\partial x}\hat{\mathbf{H}}_y - n^2\left[\frac{\partial}{\partial y}\left(\frac{1}{n^2}\frac{\partial\hat{\mathbf{H}}_y}{\partial x}\right)\right]\right\} \tag{2.43}$$

$$B_{yx}\hat{\mathbf{H}}_x = \frac{1}{2n_0k}\left\{\frac{\partial^2}{\partial x\partial y}\hat{\mathbf{H}}_x - n^2\left[\frac{\partial}{\partial x}\left(\frac{1}{n^2}\frac{\partial\hat{\mathbf{H}}_x}{\partial y}\right)\right]\right\} \tag{2.44}$$

Equations (2.29), (2.32), (2.39) and (2.40) are the full vector solutions for nonhomogeneous media. The coupling between the transverse components of the electrical and magnetic fields is taken into account in full vector solutions. However, for weakly guiding waveguides the coupling is usually weak and one can use the semi vector solutions by neglecting the coupling terms as:

$$j\frac{\partial\hat{\mathbf{E}}_x}{\partial z} = A_{xx}\hat{\mathbf{E}}_x \tag{2.45}$$

$$j\frac{\partial \hat{\mathbf{E}}_y}{\partial z} = A_{yy}\hat{\mathbf{E}}_y \tag{2.46}$$

$$j\frac{\partial \hat{\mathbf{H}}_x}{\partial z} = B_{xx}\hat{\mathbf{H}}_x \tag{2.47}$$

$$j\frac{\partial \hat{\mathbf{H}}_y}{\partial z} = B_{yy}\hat{\mathbf{H}}_y \tag{2.48}$$

In this thesis, semi vector solutions are used; since under sever bending, the coupling between the transverse components are very weak [14], also due to the iterative nature of the beam propagation method, computational cost is decreased by utilizing semi vector solutions.

Frequently in this thesis the power across the cross section is measured for different applications and it is computed in accordance with the following formula:

$$P(z) = \frac{1}{4}\int (\mathbf{E}_t^* \times \mathbf{H}_t + \mathbf{E}_t \times \mathbf{H}_t^*) \tag{2.49}$$

where, the integral is computed at the surface of the cross section.

2.3. Wide Angle Solutions

Paraxial BPM method forces small phase changes along propagation directions by forcing the second derivative to be smaller than the first derivative along z direction in Eq. (2.27). Wide angle solution which also takes into account the second derivative is useful when the waveguide makes abrupt or sudden changes along propagation direction.

In this thesis paraxial solution is used in simulations since the waveguide geometry is slowly varying along propagation directions and there are no ramps or discontinuities during propagation. But for the sake of completeness wide angle solution is presented and can be summarized as follows.

After making the slowly varying envelope approximation as in Eq. (2.27), but without ignoring the second derivative we obtain:

$$\frac{\partial^2 \hat{\mathbf{E}}_x}{\partial z^2} - 2jn_0k\frac{\partial \hat{\mathbf{E}}_x}{\partial z} - A_{xx}\hat{\mathbf{E}}_x = 0 \tag{2.50}$$

We can rearrange this equation as [15],

$$\left(\frac{\partial \hat{\mathbf{E}}_x}{\partial z} + jk(\mathbf{Z}' - 1)\hat{\mathbf{E}}_x\right)\left(\frac{\partial \hat{\mathbf{E}}_x}{\partial z} - jk(\mathbf{Z}' + 1)\hat{\mathbf{E}}_x\right) \tag{2.51}$$

Where, $\mathbf{Z}' = \sqrt{\mathbf{Z}+1}$ and $\mathbf{Z} = A_{xx}/k^2$. The first and second term of Eq. (2.51) represents the wave propagation in forward and backward direction in z direction respectively. If one is interested in forward propagation only, which is usually the case for beam propagation, the wide angle solutions can be derived as:

$$\frac{\partial \hat{\mathbf{E}}_x}{\partial z} = -jk(\mathbf{Z}^{'} - 1)\hat{\mathbf{E}}_x \tag{2.52}$$

There is no explicit solution of Eq. (2.52) because of the square root term. The general approach to overcome this problem is to approximate the square root term with polynomials. Most famous approximation is known as Pade approximation where it is defined as [16],

$$\sqrt{\mathbf{Z}+1} - 1 \approx \frac{N_m(A_{xx})}{D_m(A_{xx})} \tag{2.53}$$

where N_m and D_m are polynomials in A_{xx} of order m and n for the numerator and the denominator, respectively. Some Pade approximants that are used in BPM methods are as follows [16]:

$$Pade(1,0) : \frac{N_1}{D_0} = \frac{A_{xx}}{2} \tag{2.54}$$

$$Pade(1,1) : \frac{N_1}{D_1} = \frac{\frac{A_{xx}}{2}}{1 + \frac{A_{xx}}{4}} \tag{2.55}$$

$$Pade(1,1): \frac{N_1}{D_1} = \frac{\frac{A_{xx}}{2} + \frac{A_{xx}^2}{4}}{1 + \frac{3A_{xx}}{4} + \frac{A_{xx}^2}{16}} \tag{2.56}$$

2.4. Modes of Propagation

In order to understand the modal structure in the waveguide, we can simplify the analysis and think the problem in two dimensions where we assume an infinite slab in y direction so that electric field amplitude $\mathbf{E}_y$ is constant in y direction so that it is only a function of x and z; where z is the propagation direction. The refractive index distribution of the infinite slab can be shown in Figure 2.2. One can assume TE or TM mode of propagation for two dimensional cases. Here we analyze the TE mode where there is an infinite electrical field $\mathbf{E}_y$ in y direction.

Figure 2.2. Refractive index distribution in infinite slab waveguide

If we analyze the scalar wave equation,

$$\nabla^2 \mathbf{E}_y + n^2 k^2 \mathbf{E}_y = 0 \tag{2.57}$$

In order to solve Eq. (2.57) we make a trial solution in the form of:

$$\mathbf{E}_y(x,z) = \mathbf{E}_y(x)e^{-jn_0kz} \tag{2.58}$$

Here n_0 represents a reference refractive index. Plugging this solution into Eq (2.58) we obtain:

$$\frac{\partial^2 \mathbf{E}_y}{\partial x^2} + (n^2k^2 - n_0^2k^2)\mathbf{E}_y = 0 \tag{2.59}$$

The choice for n_0 depends on the position. For $x < 0$ and $x > d$ we choose $n = n_{clad}$ otherwise, we choose $n = n_{core}$.

We can summarize the modal structure with two different cases:

a) If $n_0 > n$ then, the transverse wave equation will have a general solution with a real exponential form:

$$\mathbf{E}_y(x) = \mathbf{E}_0 e^{\pm\sqrt{n_0^2k^2 - n^2k^2}x} \tag{2.60}$$

Where $\mathbf{E}_0$ is the electric field amplitude at $x = 0$. To be physically reasonable the negatively decaying solution is chosen for the electrical field. This solution describes the evanescent field in the waveguide where the reference refractive index is greater than the refractive index of the medium.

b) If $n_0 < n$ then, the solution has an oscillatory form as:

$$\mathbf{E}_y(x) = e^{\pm j\sqrt{n^2k^2 - n_0^2k^2}x} \tag{2.61}$$

In order to summarize the solutions in different regions it is important to describe eigenvalue of the mode as:

$$\beta = n_0 k \tag{2.62}$$

The choice of β changes the structure of the electrical field amplitude in transverse and propagation plane. Waveguides are built with $n_{core} > n_{clad}$ so that there are modes that are oscillating in core and exponentially decaying in the cladding of the waveguides. For any mode in order to have a physical solution, the necessary condition for reference refractive index is:

$$n_{clad} < n_0 < n_{core} \tag{2.63}$$

2.5. Conformal Transformations

In this thesis the bends in the waveguides are analyzed by using conformal transformations that is introduced by Mordehai et al. [17]. Conformal transformations are extensively used in image processing for mapping nonlinear geometries. The aim of conformal transformations is to change the coordinate system which contains non-linear boundaries, by a new coordinate system which can be represented by straight contours. Here a brief explanation of the theory is presented and then we show that how the transformation on the coordinate plane changes the wave equation and how can we physically interpret the transformation.

Let us analyze the conformal transformations for two dimensional scalar wave equation:

$$(\nabla^2_{x,z} + n^2(x, z)k^2)\mathbf{E}_y = 0 \tag{2.64}$$

where the waveguide is assumed to be infinite in the y direction as in previous section. If we express the transformation for the new coordinate system with complex representation:

$$a = u + jv = f(b) = f(x + jz) \tag{2.65}$$

Here f is an analytical function [18], that maps the original plane $(x+jz)$ to a new plane $(u + jv)$. Expanding with the aid of the Cauchy Riemann relations [Appendix B] where,

$$\frac{\partial u}{\partial x} = \frac{\partial v}{\partial z} \tag{2.66}$$

$$\frac{\partial v}{\partial x} = -\frac{\partial u}{\partial z} \tag{2.67}$$

we can express the wave equation in the new coordinate plane as:

$$(\nabla^2_{x,z} + \left|\frac{db}{da}\right| n^2(u(x,z), v(x,z))k^2)\mathbf{E}_y = 0 \tag{2.68}$$

Where $\left|\frac{db}{da}\right|$ is the Jacobian determinant given as:

$$\left|\frac{db}{da}\right| = \frac{1}{(\partial u/\partial x)^2 + (\partial v/\partial y)^2} \tag{2.69}$$

In Figure 2.3 ρ is the distance from the center of the bend. As an example let us consider the above index profile under the transformation:

$$a = R_2 \texttt{ln} \frac{b}{R_2} \tag{2.70}$$

This transformation maps original plane that is described in terms of x and z to a new plane that is represented by u being the distance from the center of the bend and v being the distance travel along the bend. This transformation gives:

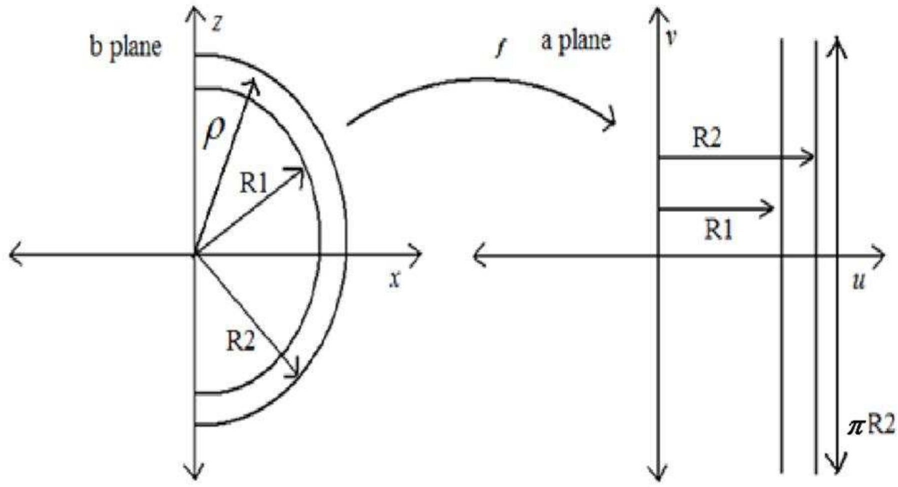

Figure 2.3. Coordinate mapping with conformal transformations

$$\left|\frac{db}{da}\right| = exp(u/R_2) \tag{2.71}$$

Equation (2.71) modifies the refractive index of the original plane as in Eq. (2.68)

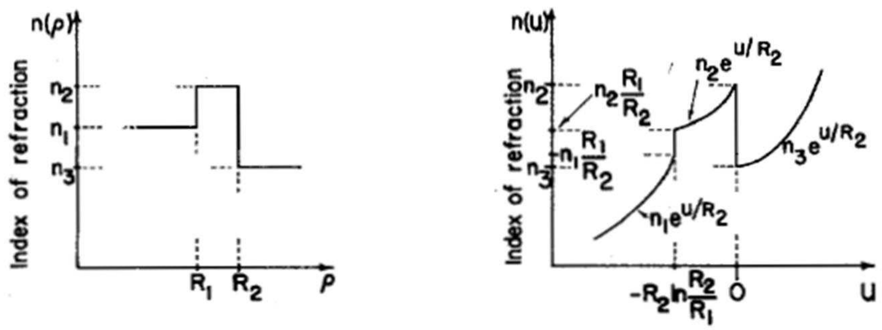

Figure 2.4. Effect of conformal transformation in refractive index

In physical terms, the refractive index increases as we move away from the center of the bend. Since the refractive index can not exceed the maximum in the waveguide the outermost point of the bend should have the index of the core. The effect of the bend is to shift the electrical field in to the bend direction where the refractive index increases. By applying conformal transformations one can analyze the curved boundaries in an unbent refractive index profile where the propagation is analyzed along the cross section of the fiber.

3. FINITE DIFFERENCE BEAM PROPAGATION METHOD

3.1. Finite Difference Approximations for Derivatives

Modeling dielectric waveguides with a step index profile is a common requirement in the design of optical devices. The interfaces between the regions of constant refractive index may generally be curved, as in a circular optical fiber, but are often composed of planar sections which themselves can either lie in an oblique direction relative to the coordinate planes or can be parallel to them, as in rectangular waveguides. Early attempts at the finite difference modeling of such structures focused mainly on the single component scalar approximation as in Eq. (2.57), which has the advantage of simplicity and computational efficiency but produces relatively accurate results only for very small index contrasts. The semi vector approximation is an advance on the scalar approximation, retaining the single component assumption, but with different interface conditions for each polarization and hence a small computational penalty due to the asymmetry of the resulting matrix.

The finite difference solution of the full vector two component formulations derived from the complete set of Maxwell's equations (equations (2.29) and (2.32)) is computationally more difficult than the single component approximations (equations (2.45) and(2.46)).

Finite difference method as its name implies carries the original problem in a discrete computational space shown as in Figure 3.1. The derivative operations are approximated by finite difference approximations. After computing the transverse derivatives, a new frame is found starting from an initial frame. Hence, the propagation is represented as frame after frame collection of electric and magnetic fields amplitudes.

The heart of the finite difference method is to approximate the derivative operators in a finite mesh. Here the finite difference approach for the semi vector equations

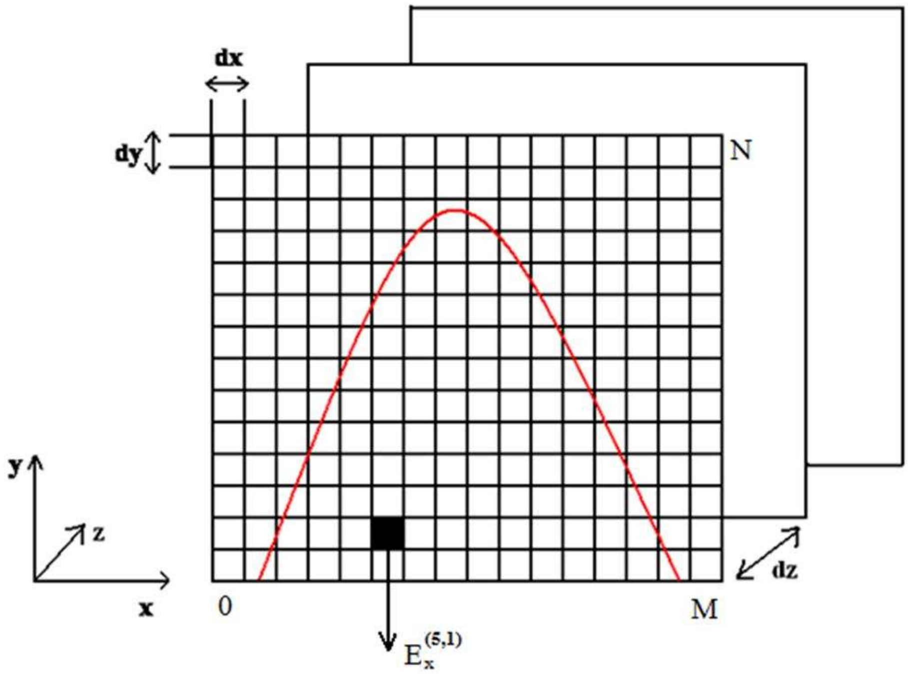

Figure 3.1. Finite difference computational space in three dimensions

are analyzed, other equations can be approximated in a similar way.

In order to represents the field elements we expand the notation of the last chapter and use subscripts to display the mesh points such as $n_{m,n}$. However since electric field intensities have subscripts representing the orientation, we add superscripts to show the mesh points.For example $E_x^{(5,1)}$ represents the element of electric field intensity in x direction sitting at the mesh as shown in Figure 3.1.

The most important term for the cause of truncation error is the first one in Eq. (2.30) and (2.33) and it can be approximated using a graded index approximation as shown in Figure 3.2, which we can explain as follows:

$$\frac{\partial}{\partial x}\left[\frac{1}{n^2}\frac{\partial}{\partial x}(n^2\mathbf{E}_x^{(m,n)})\right] \approx$$

$$\frac{\frac{1}{n^2_{(m+1/2,y)}}\frac{\partial n^2\mathbf{E}_x^{(m,n)}}{dx}\Big|_{(m+1/2,n)} - \frac{1}{n^2_{(m-1/2,y)}}\frac{\partial n^2\mathbf{E}_x^{(m,n)}}{dx}\Big|_{(m-1/2,n)}}{dx} \tag{3.1}$$

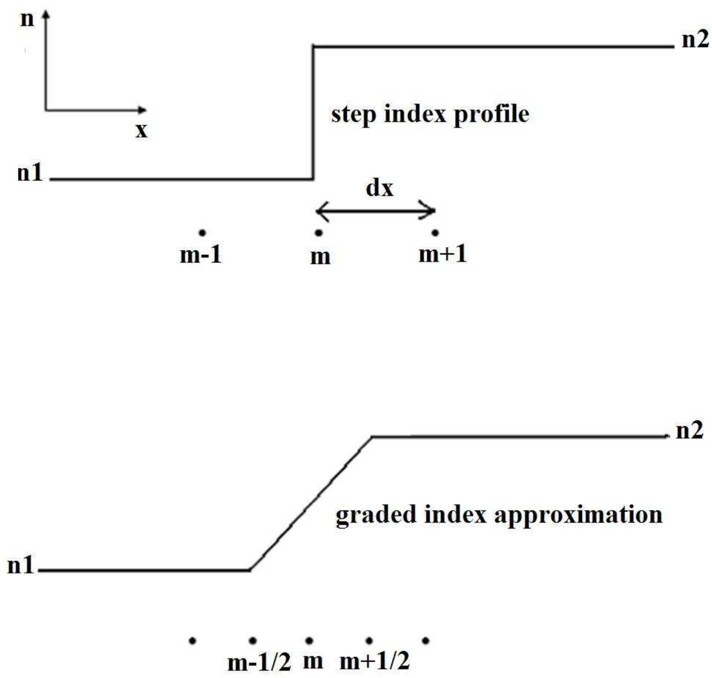

Figure 3.2. Graded index approximation to step index profile

Where,

$$\frac{1}{n^2_{(m+1/2,y)}}\frac{\partial n^2\mathbf{E}_x^{(m,n)}}{dx}\Big|_{(m+1/2,n)} \approx$$

$$\frac{2}{n^2_{(m+1,y)}+n^2_{(m,y)}}\frac{n^2_{(m+1/2,n)}\mathbf{E}_x^{(m+1,n)}-n^2_{(m,n)}\mathbf{E}_x^{(m,n)}}{dx} \tag{3.2}$$

and

$$\frac{1}{n^2_{(m-1/2,y)}}\frac{\partial n^2\mathbf{E}_x^{(m,n)}}{dx}\Big|_{(m-1/2,n)} \approx$$

$$\frac{2}{n^2_{(m-1,y)}+n^2_{(m,y)}}\frac{n^2_{(m,n)}\mathbf{E}_x^{(m,n)}-n^2_{(m-1,n)}\mathbf{E}_x^{(m-1,n)}}{dx} \tag{3.3}$$

The same approach can be applied to the first term of equation (2.34)

$$\frac{\partial}{\partial y}\left[\frac{1}{n^2}\frac{\partial}{\partial y}(n^2\mathbf{E}_y^{(m,n)})\right] \approx$$

$$\frac{\frac{1}{n^2_{(m+1/2,y)}}\frac{\partial n^2\mathbf{E}_y^{(m,n)}}{dy}|_{(m+1/2,n)} - \frac{1}{n^2_{(m-1/2,y)}}\frac{\partial n^2\mathbf{E}_y^{(m,n)}}{dy}|_{(m-1/2,n)}}{dy} \tag{3.4}$$

Where,

$$\frac{1}{n^2_{(m+1/2,y)}}\frac{\partial n^2\mathbf{E}_y^{(m,n)}}{dy}|_{(m+1/2,n)} \approx$$

$$\frac{2}{n^2_{(m+1,y)} + n^2_{(m,y)}}\frac{n^2_{(m+1/2,n)}\mathbf{E}_y^{(m+1,n)} - n^2_{(m,n)}\mathbf{E}_y^{(m,n)}}{dy} \tag{3.5}$$

and

$$\frac{1}{n^2_{(m-1/2,y)}}\frac{\partial n^2\mathbf{E}_y^{(m,n)}}{dy}|_{(m-1/2,n)} \approx$$

$$\frac{2}{n^2_{(m-1,y)} + n^2_{(m,y)}}\frac{n^2_{(m,n)}\mathbf{E}_y^{(m,n)} - n^2_{(m-1,n)}\mathbf{E}_y^{(m-1,n)}}{dy} \tag{3.6}$$

The second derivative with respect to x and y can be approximated by using a central differencing scheme given as:

$$\frac{\partial^2\mathbf{E}_x^{(m,n)}}{\partial y^2} \approx \frac{\partial}{\partial y}\left(\frac{\mathbf{E}_x^{(m,n+1/2)} - \mathbf{E}_x^{(m,n-1/2)}}{dy}\right) \tag{3.7}$$

and

$$\frac{\partial \mathbf{E}_x^{(m,n+1/2)}}{\partial y} \approx \frac{\mathbf{E}_x^{(m,n+1)} - \mathbf{E}_x^{(m,n)}}{dy} \tag{3.8}$$

$$\frac{\partial \mathbf{E}_x^{(m,n-1/2)}}{\partial y} \approx \frac{\mathbf{E}_x^{(m,n)} - \mathbf{E}_x^{(m,n-1)}}{dy} \tag{3.9}$$

resulting in

$$\frac{\partial^2 \mathbf{E}_x^{(m,n)}}{\partial y^2} \approx \frac{\mathbf{E}_x^{(m,n+1)} - 2\mathbf{E}_x^{(m,n)} + \mathbf{E}_x^{(m,n-1)}}{dy^2} \tag{3.10}$$

In order to make the computation easy, we can define the transmission and reflection coefficients for the electric field amplitudes in mesh grid at points as [20],

$$\mathbf{T}_{(m\pm1,n)} = \frac{2n^2_{(m\pm1,n)}}{n^2_{(m\pm1,n)} + n^2_{(m,n)}} \tag{3.11}$$

$$\mathbf{R}_{(m\pm1,n)} = \mathbf{T}_{(m\pm1,n)} - 1 \tag{3.12}$$

$$\mathbf{T}_{(m,n\pm1)} = \frac{2n^2_{(m,n\pm1)}}{n^2_{(m,n\pm1)} + n^2_{(m,n)}} \tag{3.13}$$

$$\mathbf{R}_{(m,n\pm1)} = \mathbf{T}_{(m,n\pm1)} - 1 \tag{3.14}$$

If we use the above coefficients for finite difference equations, we can approximate Eq. (2.30) and (2.33) as follows:

$$A_{xx}\mathbf{E}_x^{(m,n)} \approx (\frac{\mathbf{T}_{(m+1,n)}\mathbf{E}_x^{(m+1,n)} - (2 - \mathbf{R}_{(m+1,n)} - \mathbf{R}_{(m-1,n)} + \mathbf{T}_{(m+1,n)})\mathbf{E}_x^{(m,n)}}{dx^2} +$$

$$\frac{\mathbf{E}_x^{(m,n+1)} - 2\mathbf{E}_x^{(m,n+1)} + \mathbf{E}_x^{(m,n-1)}}{dy^2} + (n_{m,n}^2 + n_{0_{m,n}}^2)k^2\mathbf{E}_x^{(m,n)}) \tag{3.15}$$

and

$$A_{yy}\mathbf{E}_y^{(m,n)} \approx (\frac{\mathbf{T}_{(m,n+1)}\mathbf{E}_y^{(m,n+1)} - (2 - \mathbf{R}_{(m,n+1)} - \mathbf{R}_{(m,n-1)} + \mathbf{T}_{(m,n+1)})\mathbf{E}_y^{(m,n)}}{dy^2} +$$

$$\frac{\mathbf{E}_y^{(m+1,n)} - 2\mathbf{E}_y^{(m+1,n)} + \mathbf{E}_y^{(m-1,n)}}{dx^2} + (n_{m,n}^2 + n_{0_{m,n}}^2)k^2\mathbf{E}_x^{(m,n)}) \tag{3.16}$$

Same procedure can be applied to equation to magnetic field propagation operator in Eq. (2.41). After deriving the transverse derivatives, the derivative in the propagation direction needs to be written in finite difference form to complete the analysis. We can take the derivative in propagation direction as follows:

$$j\frac{(\mathbf{E}_x^{(m,n,l+dz)} - (\mathbf{E}_x^{(m,n,l)})}{dz} = ((1-\alpha)\mathbf{E}_x^{(m,n,l+dz)}A_{xx} - \alpha\mathbf{E}_x^{(m,n,l)}A_{xx}) \tag{3.17}$$

where α controls the stability of the derivation. As explained in [24], the case where α

equals to gives the Crank Nicholson scheme. For this scheme the resultant equations is,

$$(1 + \frac{jdzA_{xx}}{2}\mathbf{E}_x^{(m,n,l+dz)}) = (1 - \frac{jdzA_{xx}}{2}\mathbf{E}_x^{(m,n,l)}) \tag{3.18}$$

For Crank Nicholson scheme each frame is multiplied with:

$$p = \frac{1 - \frac{jdzA_{xx}}{2}}{1 + \frac{jdzA_{xx}}{2}} \tag{3.19}$$

WhereA_{xx} is computed from the current transverse plane. The magnitude of p can be easily shown to be one, implying that the Crank Nicholson scheme is unconditionally stable. the phase of p on the other hand depends on the step size dz and the propagation matrix A_{xx}. Finally we can summarize the semi vector solutions as follows.

$$(1 + \frac{jdzA_{xx}}{2}\mathbf{E}_x^{(m,n,l+dz)}) = (1 - \frac{jdzA_{xx}}{2}\mathbf{E}_x^{(m,n,l)}) \tag{3.20}$$

$$(1 + \frac{jdzA_{yy}}{2}\mathbf{E}_y^{(m,n,l+dz)}) = (1 - \frac{jdzA_{yy}}{2}\mathbf{E}_y^{(m,n,l)}) \tag{3.21}$$

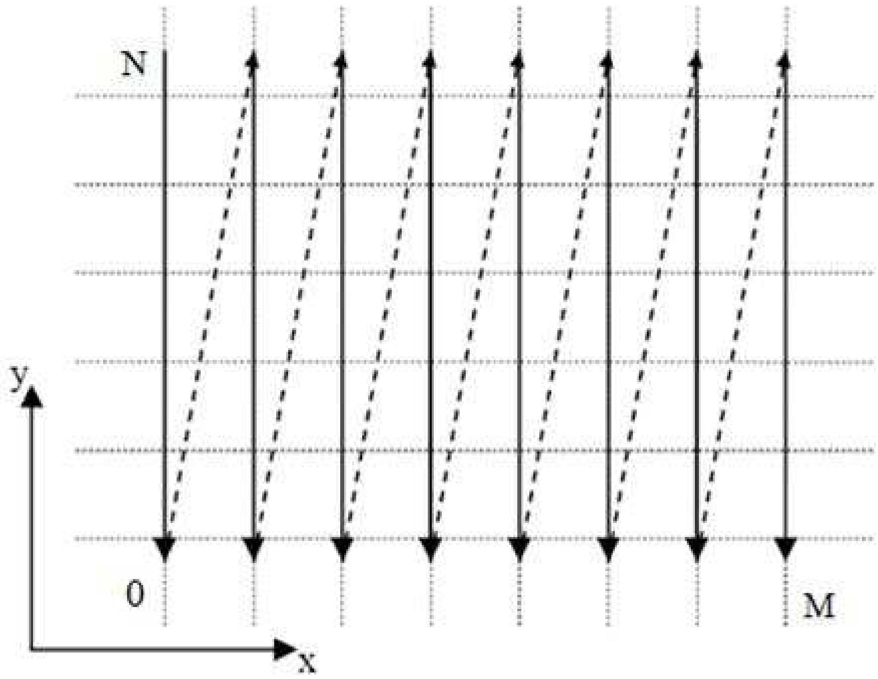

Figure 3.3. Matrix scanning procedure

3.2. Implementation

Three dimensional implementation of the finite difference beam propagation method depends on iterative matrix operation. The propagation matrix A_{xx} and A_{xx} should be constructed before starting iterations. The initial electrical field should be given as a vector in order to make calculation at each node of the mesh grid. As a result, the matrix representing the initial electrical field needs to be scanned column by column to construct a vector for iteration.

For an M by N mesh grid the resultant vector has MN elements, thus the propagation matrix A_{xx} and A_{xx} becomes MN by MN. This makes the beam propagation method computationally expensive. However propagation matrix become sparse since they have nonzero elements only around the main diagonal of the matrix. As the propagation matrix are sparse, the iteration can be solved by using explicit methods such as biconjugate gradient method [21]. This eliminates the need for LU factorization and relaxes the algorithm. After solving for the electric fields, the magnetic fields can be calculated by using curl equations in the Maxwell's equations. This provides a faster but less accurate result. A better result is to derive the finite difference operators for magnetic field as well. After obtaining electric and magnetic fields, the power across the cross section of the waveguide can be calculated in accordance with equation (2.49). An important remark we want to make is that making finite difference scheme faster or providing a better accuracy are active fields of research. Some attempts tries to approximate the transverse derivative with non iterative methods, such as split step methods [22][23]. These methods are recently reported and shown to provide faster simulation times.

3.3. Mode Solving With Imaginary Distance Method

As explained in the previous chapter, there are different modes that are propagating in the waveguide. The total light propagation is the sum of all guided modes. In order to analyze the propagation along waveguide, one has to obtain the initial electrical or magnetic field and propagation constant of that mode. Imaginary distance method is a powerful method to obtain the modes that are guided in the waveguide and in this thesis initial field amplitudes are obtained by utilizing this method. Here a brief explanation of the imaginary distance mode solving method and a two dimensional example are presented. For detail analysis one should consult the original work [24].

We can start with equation (2.45)

$$\frac{\partial \mathbf{E}_x}{\partial z} = -jA_{xx}\mathbf{E}_x \tag{3.22}$$

The solution of the above equation takes the form

$$\mathbf{E}_x(x,y,z) = e^{-jzA_{xx}}\mathbf{E}_x(x,y,0) \tag{3.23}$$

To solve the modes in the waveguide, starting from an arbitrary input field, the waveguide is assumed to be uniform in z direction so that the input field can be represented by the summation of the eigenmodes in the structure as:

$$\mathbf{E}_x(x,y,0) = \sum_{m=0}^{\infty} a_m \mathbf{E}_{x_m}(x,y) \tag{3.24}$$

where the summation includes both the guided modes and the radiation modes. The eigenvalue λ_m and the eigenvector A_{xx} of $\mathbf{E}_{x_m}(x,y)$ satisfy,

$$A_{xx}\mathbf{E}_{x_m}(x,y) = \lambda_m \mathbf{E}_{x_m}(x,y) \tag{3.25}$$

The relation between eigenvalue λ_m and the propagation constant of mode m which is denoted by β_m satisfy:

$$\lambda_m = \beta_m - n_0 k \tag{3.26}$$

where n_0 is the reference refractive index and k is the wave number in free space. By applying Taylor series expansion and using Eq. (3.25) we can write Eq. (3.26) as:

$$\mathbf{E}_x(x, y, z) = \sum_{m=0}^{\infty} a_m e^{-j\lambda_m z} \mathbf{E}_{x_m}(x, y) \tag{3.27}$$

If the field propagates along imaginary axis implying $z = j\tau$, Eq. (3.30) becomes:

$$\mathbf{E}_x(x, y, \tau) = \sum_{m=0}^{\infty} a_m e^{\lambda_m z \tau} \mathbf{E}_{x_m}(x, y) \tag{3.28}$$

If we choose n_0 equals β_0/k, then $\lambda_0 = 0$ and all other eigenvalues are negative implying that,

$$\lim_{\tau \to \infty} \mathbf{E}_x(x, y, \tau) = \sum_{m=0}^{\infty} a_0 \mathbf{E}_{x_m}(x, y) \tag{3.29}$$

This means all the higher order modes exponentially decay as the field propagates, except the fundamental mode, which remains unchanged. Thus, after propagating a certain distance, the fundamental mode will become dominant, and all the higher order modes will relatively die out. The algorithm can be used with finite difference beam propagation method where the propagation axis is made imaginary. Same procedure can be used to find the higher order modes of propagation. A detailed discussion can be found in [24].

As an example the fundematel TE mode is calculated using the finite difference

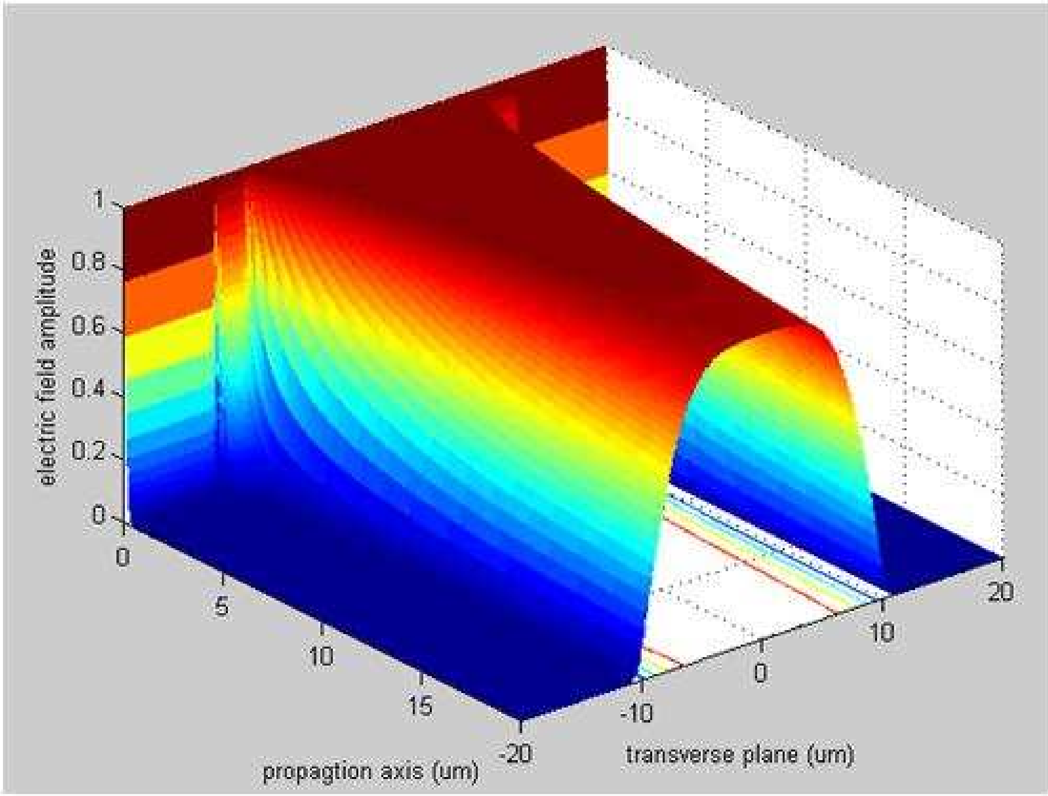

Figure 3.4. Fundamental mode emerging from an arbitrary initial field

method for a waveguide having the following parameters:

Core refractive index: 1.49

Cladding refractive index =1.403

Numerical aperture =0.5

Core width =15 um

Cladding width= 5 um

Wavelength =1 um

The step sizes are $dx = 0.1$ um $dz = 0.02$ um

3.4. Boundary Conditions

Boundary condition algorithms are very important in finite difference beam propagation method. This arises from the truncation error caused by finite mesh grid. If we think in the light of Eq. (3.11), we see that if the point lies in the left boundary one can not calculate the transmission and reflection coefficients from the neighbor points, since this is the last point on the mesh grid. In this thesis two algorithms for boundary conditions are discussed, namely Transparent Boundary Conditions (TBC) and Perfectly Matching Layers (PML). Transparent boundary conditions tries to approximate the field density at the boundary by analyzing the field behavior behind the boundary whereas the perfectly matching layer tries to add an absorbing layer along the edges so that the boundaries result in no reflection and the mesh grid seem to have extended to infinity.

3.4.1. Transparent Boundary Conditions

Transparent boundary conditions are first introduced by R. Hadley in 1992 [25]. It provides an easy solution to manipulate the edges without introducing he truncation error. Let us consider a two dimensional problem to analyze the algorithm.

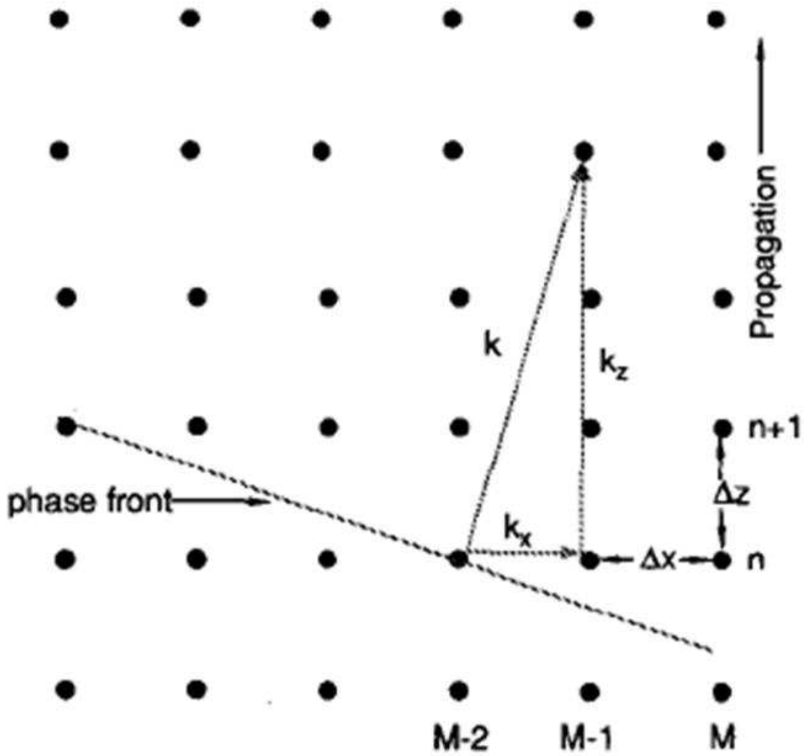

Figure 3.5. TBC algorithm

Here a phase front impinges on the right boundary. Because of the energy conservation between successive frames in finite difference approach [25], for the points at the edge of the grid, following relationship holds:

$$\frac{\mathbf{E}_x^{(M,n)}}{\mathbf{E}_x^{(M-1,n)}} = \frac{\mathbf{E}_x^{(M,n+1)}}{\mathbf{E}_x^{(M-1,n+1)}} = e^{jk_x dx} \tag{3.30}$$

The above derivation may be applied in a nearly identical manner to the left boundary. The main problem is to determine the k_x value for the boundary. The proposed solution is to observe the change around the boundary by calculating an initial k_x. Then using this value we calculate,

$$v = \frac{dz}{dx}\frac{k_x}{\sqrt{k^2 - k_x^2}} \tag{3.31}$$

where v gives us a measure of how fast the phase front impinges on the boundary. This value is rounded to the nearest integer and the next point at the boundary is approximated as:

$$\mathbf{E}_x^{(M,n+1)} = \frac{\mathbf{E}_x^{(M-v,n)}}{\mathbf{E}_x^{(M-v-1,n)}}\mathbf{E}_x^{(M-1,n+1)} \tag{3.32}$$

Initial k_x value can be easily found, if there is a priori information about the geometry of the problem. However, for problems where phase fronts are making different incident angles with boundaries, calculating initial k_x is difficult

Since, in practice the phase incident angle is not known, one has to analyze many points inside the boundary and approximate the phase incident angle and . On the other hand due to the simplicity of TBC algorithm, it is commonly used in applications when there is less radiation to the outside from the boundary or the incident angles on the boundaries can be approximated. For analyzing waveguides with considerable radiation and complex geometries a more powerful boundary method is needed and Transparent Boundary Conditions prove to be inadequate.

3.4.2. Perfectly Matching Layers

Perfectly matched layers method approaches to the boundary conditions problem at a different way. Berenger showed that [24], utilizing a buffer absorbing layer called perfectly matching layer, it is possible to capture and dissipate all the radiation into the absorbing layer. As a result, the truncation error caused by the boundaries in the finite difference scheme is solved since the boundaries are viewed to have extended to infinity.

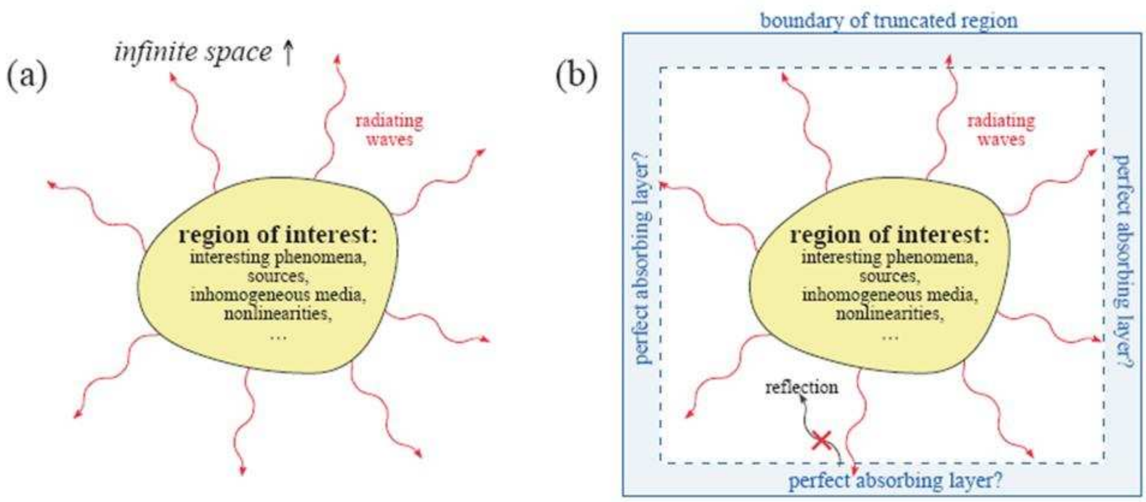

Figure 3.6. PML approach a) physical space b) finite computational space

When a wave enters the absorbing layer, it is attenuated by the absorption and decays exponentially; even if it reflects off the boundary of the computational space, the returning wave after one round trip through the absorbing layer is exponentially tiny. The problem with this approach is that, whenever you have a transition from one material to another, waves generally reflect, and the transition from non absorbing to absorbing material is no exception, so instead of having reflections from the grid boundary, we now have reflections from the absorber boundary. However, Berenger showed that a special absorbing medium could be constructed so that waves do not reflect at the interface. Although PML was originally derived for the Maxwell's equations, the same ideas are immediately applicable to other wave equations.

The main theory behind the perfectly matching layers is complex coordinate stretching. It can be explained by a simple example:

If we consider the function $E = e^{jkx}$, where $k = 2\pi\lambda$ and evaluate this function for positive x, we see that the function is oscillatory if x is real. However if we modify x and force it to have an imaginary part after 3 wavelength, the resultant function does not changes for points before 3 wavelength; yet it exponentially decays with the imaginary part of x.

The power comes from the analytical continuity [18] of the function $E = e^{jkx}$. It does not matter if it is evaluated as real or imaginary x, the function will be continuous as long as x is continuous. The region where x has imaginary part acts as a dissipative medium for the function. However, this artificial medium does not cause any reflections and does not alter the field behavior outside the absorbing region.

The following example is nothing but complex coordinate transformations for certain regions of interest. Perfectly matching layers resemble the idea of imaginary distance propagation for mode solving, since it takes the advantage of the continuity of the equations and exponentially decaying nature of wave solutions under propagation over complex axis. In order to apply this idea, we can analyze Maxwell equations in a new space transformed from the original space with the transformation,

$$\hat{x}(x) = x + jf(x) \tag{3.33}$$

Where f function tells us how we deform the contour along x. The derivative with respect to x is calculated as:

$$\frac{\partial \hat{x}}{\partial x} = 1 + j\frac{\partial f(x)}{\partial x} \tag{3.34}$$

The derivation made by Berenger uses [24],

$$\frac{\partial f(x)}{\partial x} = \frac{\sigma(x)}{\omega} \tag{3.35}$$

Where $\sigma(x)$ is the conductivity of the medium and it is zero in the region of interest and nonzero in the perfectly matching layer. In physical terms, the conductivity associated with perfectly matching layers makes these regions dissipative so that the field exponentially decays. This transforms the derivative in the Maxwell's equations as:

$$\frac{\partial f(x)}{\partial x} \rightarrow \frac{1}{1 + j\frac{\sigma_x(x)}{\omega}}\frac{\partial}{\partial x} \tag{3.36}$$

The phase velocity is used in order to provide equal attenuation for waves having different wavelengths, as can be seen from the original function evaluated with new transformation:

$$e^{jk_{\hat{x}}} = e^{jk_x} e^{\frac{k}{\omega}\int \sigma_x(x)dx} \tag{3.37}$$

Here the attenuation is independent of wavelength since equal to the inverse of the speed of light.

The PML approach seems perfect as it is easy to apply. It does not need special care for implementation and it can be applied to different propagation schemes with no modification. Along with its advantages the PML approach carry some disadvantages. We can summarize the limitations of the PML as follow:

a) Discretization and numerical reflections:

PML is only reflectionless when solving the exact wave equations. As soon as we discretize the problem (whether for finite difference or finite element methods), we are only solving an approximate wave equation and the analytical perfection of PML is no longer valid. PML is still an absorbing material that is, the waves that propagate within it are still attenuated, even discrete waves. The boundary between the PML and the regular medium is no longer reflectionless, but the reflections are small because the discretization is hopefully a good approximation for the exact wave equation. Reflections can be made arbitrarily small as long as the medium is slowly varying. In practice the conductivity starts slowly to increase from zero to a maximum at the boundary as quadratic or cubic functions. This way the reflections at the beginning of PML region and at the boundaries can be made very small.

b) Angle dependent absorption:

The field amplitude decrease more as it propagates in the PML region. For waves that are parallel or making small angles with the PML region the decay is low. However, in a three dimensional problem, if the geometry is not very complex, these waves will hopefully hit on another PML region without changing the field of interest, and they will eventually decay.

4. Bend Enhanced Optical Touch Sensor Analysis

The power loss calculation formulas in the literature [26][27][28][29][30], address the power attenuation under slight bends only and they assume an infinite cladding so that no power couples back from the cladding in to the core. However, sensor applications treats the cladding as a power exchange layer, where certain amount of power is coupled to the cladding for getting information from the medium that the cladding interacts. Our aim in the following simulations is to analyze the amount of power that is coupled to the cladding, radiated to the outside of the waveguide with and without any contact medium and analyze the touch sensing capabilities of the bend enhanced optical touch sensor.

We have constructed a three dimensional finite difference beam propagation method using paraxial, semi vector solutions. The bending simulations are performed for a waveguide having 30 um core and 40 um total diameter. The numerical aperture of the fiber is chosen to be 0.5, which is the case for most of the plastic optical fibers, and its core and cladding refractive indeces are 1.49 and 1.403 respectively. The wavelength of the beam is chosen to be 950 nm. The finite difference scheme is applied with step sizes of $dx = 0.2$ um $dy = 0.2$ um, $dz = 0.2$ um. First the step size along propagation is chosen to be 0.1 um but making it 0.2 um did not affect he stability and accuracy of the program. The mesh grid for the transverse plane is chosen to be 30 um by 30 um. This means at each frame the electric and magnetic field vectors are represented by 300 by 300 matrices and the propagation matrix A_{xx} and A_{yy} in Eq. (3.23) and Eq. (3.24) become 90000 by 90000.

We should note that the dimensions chosen for the simulations are not practical since the smallest waveguides that are used today have 50 um core diameter. Since we have performed several simulations for different setups, the simulation times and the amount of obtained data become huge. However for an optimum design a detailed simulation can be performed to analyze a real optical fiber geometry. Here our intention is to show the effect of bending and coupling on a theoretical small scale setup.

At the edges of the mesh grid we have applied a PML region having a quadratic form:

$$\sigma(x,y) = \sigma_{max}(\frac{xdist}{pmllength} + \frac{ydist}{pmllength})^2 \tag{4.1}$$

where, σ is the conductivity of the PML region, σ_{max} is the maximum conductivity being 0.1 (mho/m) , $pmllength$ is chosen to be 5 um and $xdist$ and $ydist$ are the distance from the boundary for the x and y dimensions respectively.

4.1. Mode Solving

We have applied the imaginary distance method as explained in Chapter 3 in order to solve for the fundamental mode in the waveguide. Since the beam propagation method is computationally expensive, throughout our simulation, we have used fundamental mode only. As explained in [17] when an optical waveguide is bent severely, the higher order modes decays faster than the lower order modes; however, one can build sensors utilizing the lower order modes. Our aim is to analyze the power of the fundamental mode and show its change for different setups. In a similar way one can derive the higher order modes and make a more detailed analysis.

We have started from an arbitrary electrical field and propagated the beam along the waveguide. We have observed that initial field has converged to the fundamental mode for a reference refractive index $n_0 = 1.49$ after propagation the field for 800 um.

For all bending simulations the fundamental mode of the electrical fields $\mathbf{E}_x$ and $\mathbf{E}_x$ are propagated, then the corresponding magnetic fields are calculated from the electrical fields by using Eq. (2.1). Then we have calculated the power in the cross section of the fiber using Eq. (2.49). The PML regions have successfully absorbed the outgoing radiation for different bending setup.

4.2. Constant Bending

We have propagated the beam under constant bending for different bend radii and observed the beam for the simulated radius. Then we have analyzed the power loss, the amount of power coupled to the cladding and the power confined in the core. At the end of each simulation we have given our results in tabular form and made comments. Figure 4.1 shows the geometry that is used in our simulations:

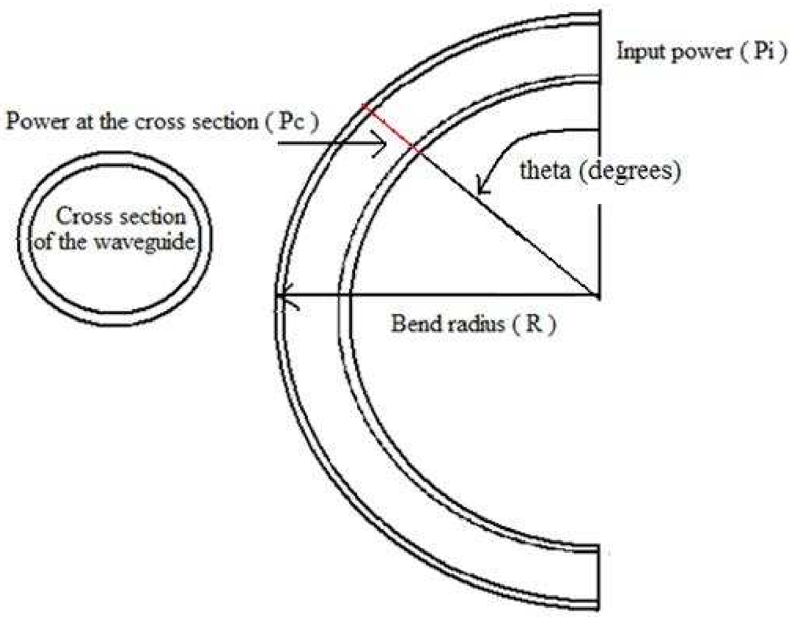

Figure 4.1. Geometry used in the simulations

We have analyzed the normalized power change in the core and cladding across the cross section of the waveguide as a function of theta (plane angle of the cross section) for 4 different bend radii with the intention of finding the effects of power coupling in the layers of the waveguide. We have also observed the stability of finite difference scheme and Perfectly Matching Layers. Even under severe bending conditions we have observed that the radiated power is easily absorbed in the PML region with negligible reflections from the boundaries.

As can be seen from Figure 4.2 the effect of bending causes the power to oscillate between core and cladding in the waveguide and it exponentially approaches a limit. However the first half turn in the waveguide can be used as a sensor since a considerable

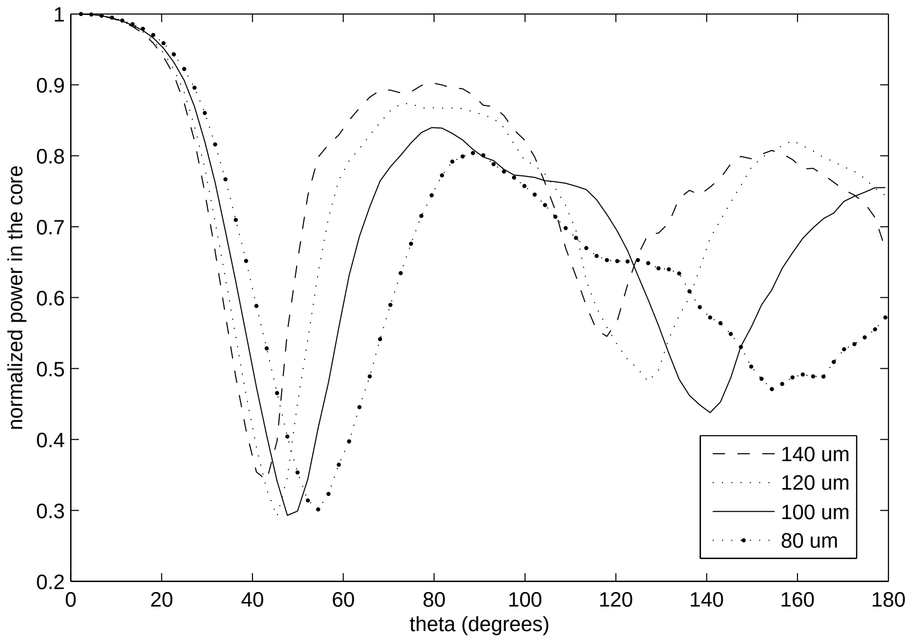

Figure 4.2. Normalized power in the core across the cross section for different bend radii

amount of power is transferred to the cladding.

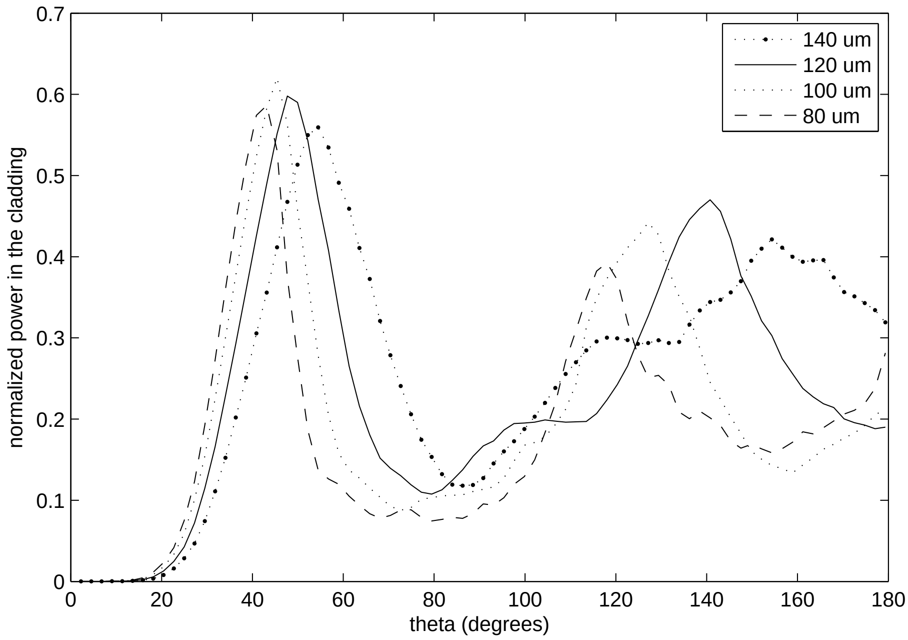

Figure 4.3. Normalized power in the cladding across the cross section for different bend radii

We observed that the peak power in the cladding makes a maximum for 100 um and 120 um bend radii and it becomes less whether we increase or decrease the bend radius.

Table 4.1. Constant bending simulation results

	Bending Radius (um)			
	80	100	120	140
Peak Power in the cladding	0.563	0.602	0.626	0.590
Power in the core after one half turn	0.582	0.760	0.742	0.768
Power in the cladding after one half turn	0.314	0.191	0.219	0.208
Power loss after one half turn	0.104	0.051	0.039	0.024

Table 4.1 gives the results for bending simulations. As we can see the amount of power loss increases as we decrease the bending radius. These plots will become important when we analyze the behavior of the waveguide with a contact medium on the cladding

4.3. Touching The Bent Waveguide

Having analyzed the change of power in the waveguide under different bending conditions, we now show the effect of touching the bent waveguide that is bringing a contact medium next to the cladding. Again we make our analysis for one half turn only. During our simulations we have simulated the human skin with a medium having refractive index of 1.4, 1.45 and 1.5. This medium is brought in close contact with the bent waveguide and allowed to continuously touch the surface of the waveguide at one point only.

After making the touch simulations for contact medium having different refractive indeces, we have seen that changing the refractive index of the contact medium between 1.4 and 1.5, did not affect the power loss considerably. So we have used a refractive index of 1.4 for the contact medium to model the touching on the waveguide.

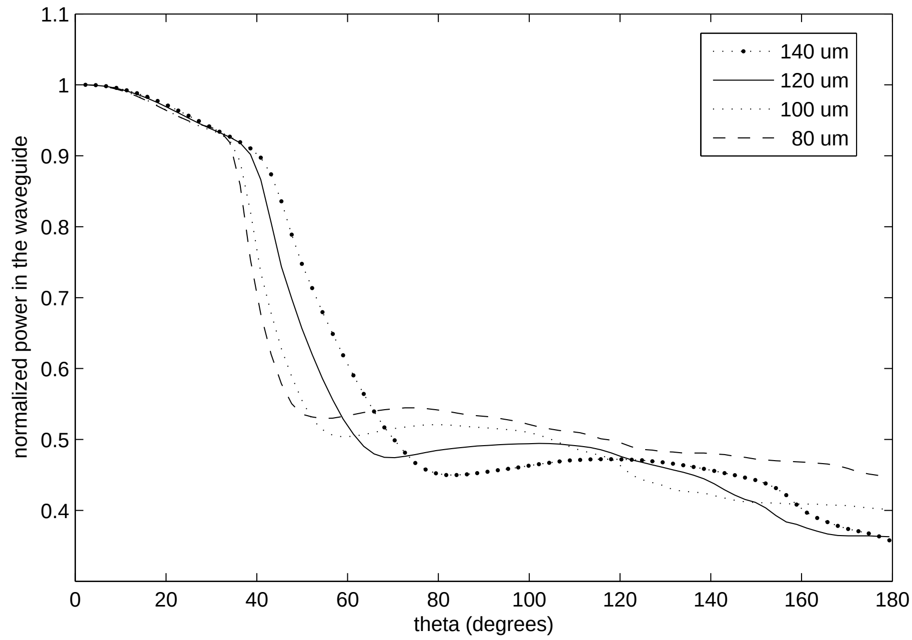

Figure 4.4. Normalized power in the waveguide cross section for different bend radii, in case of touching

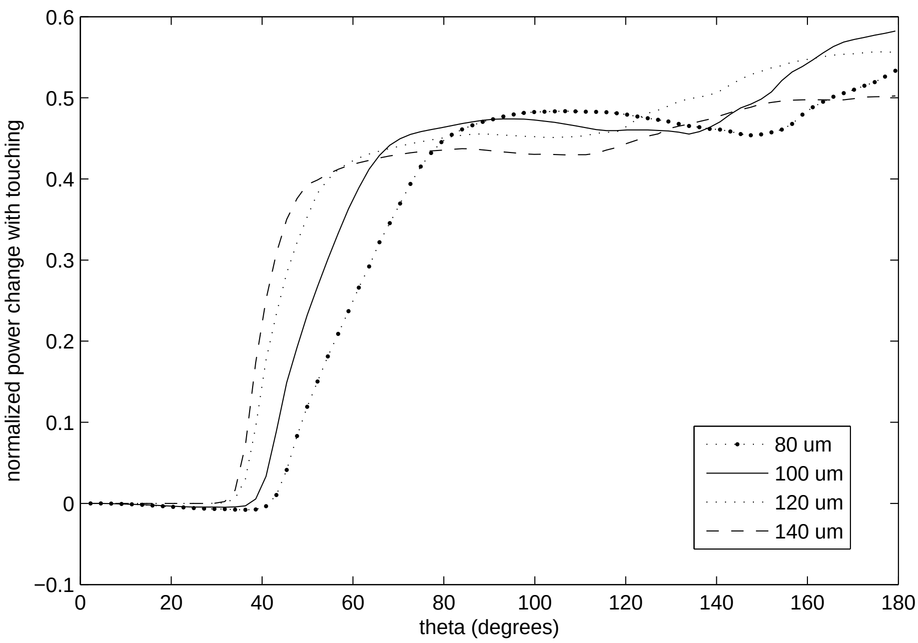

Figure 4.5. Normalized power change at the cross section of the waveguide for different bend radii, in case of touching

As can be seen from the results at all cases the power decreases considerably meaning the waveguide can detect the presence of touching even if the contact point

Table 4.2. Touch sensing simulation results

	Bending Radius (um)			
	80	100	120	140
Power change with touching	0.540	0.587	0.559	0.505
Power in the core after one half turn	0.169	0.30	0.311	0.351
Power in the cladding after one half turn	0.187	0.064	0.091	0.097
Power loss after one half turn	0.664	0.636	0.598	0.552

is very small.

4.4. Results

As can be seen from the above tables and plots, for all cases the touching of the waveguide can be detected by monitoring the power change at the cross section of the waveguide. For the analyzed refractive index profile we observe that the optimum bend radius that causes the maximum power change in the waveguide with the touching is around 100 um. Since for this case the amount of power coupled to the cladding is maximum.

One important result is the peak power we can achieve in the bent waveguide when there is no touching. The amount of peak power in the cladding gives us the sensing capabilities of the waveguide. As we have seen from the plots, peak power in cladding is reached for 100 um and 120 um cases and for these bend radii the amount of detectable power change is also maximum. We reason that the amount of peak power that can be coupled into the cladding changes with different bend radii. However there is an optimum point where it reaches a maximum and for this bend radius the touch sensing capability is maximum as well. We can summarize the results of our simulations as follows:

- We have showed the correct operation of our three dimensional finite difference beam propagation method that adopts conformal transformations to analyze the curved boundaries of the waveguides.

- Perfectly matching layer boundary conditions showed negligible amount of power reflection from the boundaries even in the case of considerable amount of power radiation from the finite difference mesh. This can be clearly observed from the plots. For example even for the case of 80 um bending, almost 66 percent of the power in the waveguide is radiated to the outside without any reflections.

- As an application we have demonstrated a novel touch sensor approach and observed that it has a good touch sensing capability. We have shown that under considerable bending the presence of human touch decreases the amount of power in the waveguide and this power change can be used as a touch sensor

- Generally, for sensor applications we have shown that the amount of peak power that can be transferred to the cladding during one half turn gives a measure of the sensing capability of the waveguide.

For our proposed touch sensor, we can summarize its advantages and its possible use as follows:

- Bend enhanced optical touch sensor is immune to electromagnetic interference because the sensing occurs in optical frequencies.

- It requires small activation forces since only a tipping on the surface becomes enough for sensing.

- Since the sensor does not contain any moving parts it is highly durable.

- The sensor can be made transparent by properly processing the waveguide and it can be used together with display systems as well. Since the infrared light beam is propagating in the waveguide the sensing will not be observed by the human eye.

- By utilizing the analyzed half turn bend enhanced touch sensors in a grid where each grid having one half bend as a sensitive point, it can be used as a two dimensional touch sensor.

5. CONCLUSIONS

We have explained the methodology of the finite difference beam propagation methods to analyze bending and coupling losses in a plastic optical fiber waveguide. The curved geometries are simulated with Conformal Transformations so that the refractive index distribution is modified rather than its orientation. Our analysis method has been proved to be functional even in the case of a considerable radiation to the outside of the waveguide and unwanted reflections from the wall are shown to be eliminated by the perfectly matching layers. One drawback of our analysis method is being paraxial. By using a higher order Pade approximation it can analyze complex geometries,for example, abrupt changes in the propagation direction, rib waveguides and arrayed waveguide gratings. Since for the simulation of bend enhanced touch sensor it was not needed, we leave its implementation as a future work.

As for the bend enhanced touch sensor, we have demonstrated the characteristic of power oscillation between core and cladding for different bend radii. We have shown that the cladding can allow power coupling in order to sense the presence of a human touch. Our simulation results showed that the ratio of the peak power that can be coupled to the cladding gives a measure for the sensing capabilities of the waveguide. We have analyzed different bend radii and showed there is an optimum bend radius for the waveguide during one half turn where it can efficiently detect the presence of a contact to the cladding.

APPENDIX A: FORMULAS USED IN THE THESIS

Gradient, of scalar function $f(x, y, z)$ represents a vector field given by:

$$\nabla f = (\frac{\partial f}{\partial x}, \frac{\partial f}{\partial y}, \frac{\partial f}{\partial z}) \tag{A.1}$$

Divergence, of a continuously differentiable vector field $\mathbf{F} = F_x\mathbf{i} + F_y\mathbf{j} + F_z\mathbf{k}$ is a scalar field given by:

$$\nabla \cdot \mathbf{F} = \frac{\partial F_x}{\partial x} + \frac{\partial F_y}{\partial y}, \frac{\partial F_z}{\partial z} \tag{A.2}$$

Laplacian in Euclidean space is defined as the divergence of gradient of a vector field given $f(x, y, z)$ as:

$$\Delta f = \frac{\partial^2 f}{\partial x^2} + \frac{\partial^2 f}{\partial y^2}, \frac{\partial^2 f}{\partial z^2} \tag{A.3}$$

Vector Laplacian of a vector field $\mathbf{F} = F_x\mathbf{i} + F_y\mathbf{j} + F_z\mathbf{k}$ in Euclidean Space is given by:

$$\Delta^2 f = (\delta F_x, \delta F_y, \delta F_z) \tag{A.4}$$

APPENDIX B: DERIVATION OF CAUCHY RIEMANN EQUATIONS

If we let:

$$a = u + jv = f(b) = x + jz \tag{B.1}$$

where,

$$b = x + jz \tag{B.2}$$

we can take the derivative as:

$$db = dx + jdz \tag{B.3}$$

the elements of the original plane can be expresses in terms of the complex variable b as:

$$x = \frac{b + \bar{b}}{2} \tag{B.4}$$

Where $\bar{b}$ is the complex conjugate of b similarly,

$$z = \frac{b + \bar{b}}{2j} \tag{B.5}$$

We can take the derivatives as:

$$\frac{\partial x}{\partial b} = \frac{1}{2} \tag{B.6}$$

$$\frac{\partial z}{\partial b} = \frac{1}{j2} \tag{B.7}$$

The derivative of the coordinate transformation function f with respect to complex variable b can be written in terms of coordinate axis x and z and the function f as:

$$\frac{\partial f}{\partial b} = \frac{\partial f}{\partial x}\frac{\partial f}{\partial b} + \frac{\partial f}{\partial z}\frac{\partial f}{\partial b} \tag{B.8}$$

By using Eq. (B.6) and (B.7) in Eq. (B.8) we obtain:

$$\frac{\partial f}{\partial b} = \frac{1}{2}(\frac{\partial f}{\partial x} - j\frac{\partial f}{\partial z}) \tag{B.9}$$

We can express Eq. (B.9) in terms of u and v as:

$$\frac{\partial f}{\partial b} = \frac{1}{2}\left[(\frac{\partial u}{\partial x} + j\frac{\partial v}{\partial x}) - j(\frac{\partial u}{\partial z} + j\frac{\partial v}{\partial z})\right] \tag{B.10}$$

Along real x axis we have $\partial f \partial z = 0$,

$$\frac{\partial f}{\partial b} = \frac{1}{2}(\frac{\partial u}{\partial x} + j\frac{\partial v}{\partial x}) \tag{B.11}$$

Along imaginary x axis we have $\partial f \partial x = 0$,

$$\frac{\partial f}{\partial b} = \frac{1}{2}(-j\frac{\partial u}{\partial z} + \frac{\partial v}{\partial z}) \tag{B.12}$$

If f is complex differential above two equations must be equal so:

$$\frac{\partial u}{\partial x} = \frac{\partial v}{\partial z}, \frac{\partial v}{\partial x} = -\frac{\partial u}{\partial z} \tag{B.13}$$

REFERENCES

1. Scarmozzino R., "Numerical Techniques for Modeling Guided Wave Photonic Devices", *IEEE Journal Of Selected Topics In Quantum Electronics*, Vol. 6, No. 1, January 2000.

2. Brosig J. A., "Spatial Frequency-Based Micro-bending Fiber Optic Sensor", *IEEE International Frequency Control Symposium*, 1995.

3. Kodl G., "A New Optical Waveguide Pressure Sensor Using Evanescent Field", *Electronic Components and Technology Conference*, 2004.

4. Jefferson Y. H., "Low-Cost Multi-Touch Sensing through Frustrated Total Internal Reflection", *Media Research Laboratory New York University*, October 23-27, 2005.

5. Izadi S., S. Hodges, A. Butler, A. Rrustemi and B. Buxton, "ThinSight: Integrated Optical Multi-touch Sensing through Thin Form-factor Displays", *EDT 2007, San Diego, California*, August 2007.

6. Obayya S. A., M. A. Rahman, "Full Vectorial Finite-Element-Based Imaginary Distance Beam Propagation Solution of Complex Modes in Optical Waveguides", *Journal of Lightwave Technology*, Vol. 20, No. 6, June 2002.

7. Saitoh K., "Full-Vectorial Finite Element Beam Propagation Method with Perfectly Matched Layers for Anisotropic Optical Waveguides", *Journal of Lightwave Technology*, Vol. 19, No. 3, March 2001.

8. Obayya S. A., M. A. Rahman, "Finite Element Based Beam Propagation Modal Solution of Optical Waveguide Problems", *IEEE MTT-S Digest*, 2004.

9. Buxton W., "Issues and Techniques in Touch-Sensitive Tablet Input", San Fransisco July 22-26 Volume 19, Number 3, 1985.

10. So-Ling C., L. Li, “A Multi-Layered Reflection Model of Natural Human Skin”.

11. Pollock C. R., “Fundamentals of Optoelectronics”, pp. 13, Irwin Press, 1995.

12. Pollock C. R., “Fundamentals of Optoelectronics”, pp. 17, Irwin Press, 1995.

13. Huang W. P., “Simulation of Three Dimensional Optical Waveguides by a Full Vector Beam Propagation Method“, *IEEE Journal of Quantum Electronics*, Vol. 29, No.10 , October 1993.

14. Schermer R. T., “Improved Bend Loss Formula Verified for Optical Fiber by Simulation and Experiment”, *IEEE Journal of Quantum Electronics*, Vol. 43, No. 10, October 2007.

15. Flamino R. S., C. C. Amlcar and B. V. Borges, “Improved Wide-Angle Finite-Difference Beam Propagation Method for the Analysis of Nonlinear Optical Waveguides”, *IEEE Transactions on Magnetics*, Vol. 38, No. 2, March 2002.

16. Ilic I., “Investigation of the Pade Approximant Based Wide-Angle Beam Propagation Method for Accurate Modeling of Waveguiding Circuits”, Journal of Lightwave Technology, Vol. 14, No. 12, December 1996.

17. Heiblum M., “Analysis of Optical Waveguides by Conformal Transformation”, *IEEE Journal of Quantum Electronics*, Vol. QE-11, NO. 2, February 1975.

18. http://en.wikipedia.org/wiki/Analytic function.

19. http://mathworld.wolfram.com/Cauchy-RiemannEquations.html.

20. Huang W. P., “Simulation of Three-Dimensional Optical Waveguides by a Full-Vector Beam Propagation Method”, *IEEE Journal of Quantum Electronics*, Vol. 29, No. 10, October 1993.

21. Matlab v7.1 Help.

22. Sharma A., "A New Finite Difference Based Method for Wide Angle Beam Propagation", *IEEE Photonics Technology Letters*, Vol. 18, No. 8, April 15, 2006.

23. Feng N. N., G. Zhou and W. Huang, "An Efficient Split-Step Time-Domain Beam-Propagation Method for Modeling of Optical Waveguide Devices", *ournal Of Lightwave Technology*, Vol. 23, No. 6, June 2005.

24. Xu C. L. , W. P. Huang, "Efficient and Accurate Vector Mode Calculations by Beam Propagation Method", *Journal of Light wave Technology*, Vol. 11, No. 7, July 1993.

25. Hadley G. R., "Transparent Boundary Condition for the Beam Propagation Method", *IEEE Journal of Quantum Electronics*, Vol. 28, No. I, January 1992.

26. Berenger J. P., "Perfectly Matched Layer for the FDTD Solutions of Wave Structure Interaction Problems", *IEEE Transactions On Antennas and Propagation*, Vol. 44, No. 1, January 1996.

27. Badar A. H., T. S. Maclean, "Radiation from circular bends in multimode and single-mode optical fibres", *IEE Proceedings*, Vol. 136, Pt. J , No. 3, June 1989.

28. Andreasen S. B., "New Bendings Formula Explaning Bends on Loss Curve", *Electronic Letters 8th October*, Vol. 23 No. 21, 1987.

29. Harris A. J. and P. F. Castle, "Bend Loss Measurements on High Numerical Aperture Single-Mode Fibers as a Function of Wavelength and Bend Radius" , *Journal Of Lightwave Technolog*, VOL. LT 4, NO. 1 , January 1986.

30. Winkler C. , "Power Attenuation in Bent Parabolic index Slab and Fiber Waveguides", *Electronic Letters 8th October*, Vol. 14 No.17, 1987.

31. Arrue J., J. Zubia, G. Durana and J. Mateo, "Parameters Affecting Bending Losses in Graded-Index Polymer Optical Fibers", *IEEE Journal On Selected Topics In Quantum Electronics*, Vol. 7, No. 5, September 2001.

32. Faustini L. and G. Martini, "Bend Loss in Single-Mode Fibers", *Journal of Light wave Technology*, Vol. 15, No. 4, April 1997.